Modeling Holes and Inclusions by Level Sets in the Extended Finite Element Method

N. Sukumar[1,*] D. L. Chopp[2] N. Moës[3] T. Belytschko[3]

[1] Department of Civil Engineering, Northwestern University, Evanston, IL 60208

[2] Department of Engineering Sciences and Applied Mathematics, Northwestern University, Evanston, IL 60208

[3] Department of Mechanical Engineering, Northwestern University, Evanston, IL 60208

Accepted for publication in *Computer Methods in Applied Mechanics and Engineering*, November 2000

Abstract

A methodology to model arbitrary holes and material interfaces (inclusions) without meshing the internal boundaries is proposed. The numerical method couples the level set method (Osher and Sethian, 1988) to the eXtended Finite Element Method (X-FEM) (Moës et al., 1999). In the X-FEM, the finite element approximation is enriched by additional functions through the notion of partition of unity. The level set method is used for representing the location of holes and material interfaces, and in addition, the level set function is used to develop the local enrichment for material interfaces. Numerical examples in 2-dimensional linear elastostatics are presented to demonstrate the accuracy and potential of the new technique.

KEYWORDS: Extended Finite Element Method, level set method, voids, material interface, elastic inclusion

*Corresponding author: Princeton Materials Institute, 416 Bowen Hall, Princeton University, Princeton, NJ 08544-5263. Tel.: +1-609-258-0494, E-mail: nsukumar@princeton.edu

1 Introduction

Defects such as pores, cracks, and inclusions are important to the structural integrity and durability of components. For example, material interfaces in composites are modeled to predict the mechanical behavior and to establish macroscopic material properties. The accurate modeling of voids and inclusions is hence of interest to both the theorist and the practitioner. In finite element methods, the mesh is required to conform to internal boundaries in the model. Although mesh generation is very well-established in 2-dimensions, meshing arbitrary number and distribution of defects and inclusions is still a time-consuming and burdensome task.

In this paper, we describe the modeling of internal boundaries from a different viewpoint, by using the level set method within the framework of the eXtended Finite Element Method (X-FEM) (Moës et al., 1999). In the extended finite element method, the finite element approximation is enriched by additional functions through the notion of partition of unity (Melenk and Babuška, 1996). The recognition and use of partition of unity enrichment strategy to solve boundary-value problems with internal boundaries is due to Oden and co-workers (Oden et al., 1996; Oden et al., 1998; Duarte et al., 1998; Duarte et al., 2000)—the numerical technique was coined as the Generalized Finite Element Method (GFEM). Strouboulis et al. (2000) used local enrichment functions in the GFEM for modeling re-entrant corners in 2-dimensions, and in Strouboulis et al. (2000), enrichment functions for holes are proposed.

In the X-FEM, the additional functions are used to model cracks, voids or inhomogeneities, and also to improve accuracy in problems where some aspects of the functional behavior of the solution field are known *a priori*. As opposed to the GFEM in which the analytical solution of a given boundary-value problem is embedded into the finite element space, in the X-FEM the proximity to the finite element method is consistently sought by carrying out only the requisite enrichment to model the internal boundary (crack or inclusion) of interest. The GFEM is amenable to accurate numerical solutions with coarse meshes and provides the capability of p-type adaptivity. In the X-FEM, less dependence on known closed-form solutions is emphasized which provides for greater flexibility to solve a wider range of problems. For a few applications in the above spirit, see Moës et al. (1999) and Dolbow et al. (2000) for crack modeling in 2-dimensions, and Sukumar et al. (2000) and Sukumar et al. (2000) for three-dimensional elastostatics and fatigue crack growth modeling.

The level set method is a numerical technique for tracking moving interfaces (Osher and Sethian, 1988). The evolving interface is represented as the zero level set of a function of one higher dimension (i.e., $\varphi(\mathbf{x}, t) = 0$). The motion of the interface is embedded in a hyperbolic equation in terms of $\varphi(\mathbf{x}, t)$. In this paper we pursue 2-dimensional elastostatic applications, and hence the interface is static. The interface for geometric entities such as holes and inclusions is represented by the level set function. In addition, using φ, the local enrichment function for material interfaces is constructed.

The outline of this paper follows. In the next section, we give a brief introduction to the eXtended Finite Element Method, and in Section 3, the level set method is introduced. In Section 4, the modeling of voids and inclusions is addressed. The strong and weak forms of the Galerkin method for 2-dimensional elastostatics, along with the discrete equations for the X-FEM are given in Section 5. In Section 6, two different approaches for the numerical integration of the weak form are described. Numerical results are presented in Section 7, and we close with some concluding remarks in Section 8.

2 The Extended Finite Element Method

In the finite element method, the presence of flaws or inhomogeneities such as cracks, voids, and inclusions must be taken into account in the mesh generation process—the edges of the element must conform to these geometric entities.

The eXtended Finite Element Method aims to alleviate much of the burden associated with mesh generation for problems with voids and interfaces by not requiring the finite element mesh to conform to internal boundaries. The essence of the X-FEM lies in sub-dividing a model into two distinct parts: mesh generation for the domain (excluding internal boundaries); and enriching the finite element approximation by additional functions that model the internal boundaries.

Consider a domain $\Omega \subset \mathbb{R}^2$ which is partitioned into finite elements, and let $\mathbf{N} = \{n_1, n_2, \ldots, n_m\}$ be a set of m nodes in the mesh. In addition, let $\Omega_g \subset \Omega$ be a region for which some enrichment is required. For a material interface, the domain Ω_g is the curve representing the material interface and in the case of a void, Ω_g is the region occupied by the void. The X-FEM displacement approximation assumes the general form:

$$\mathbf{u}^h(\mathbf{x}) = \sum_{\substack{I \\ n_I \in \mathbf{N}}} \phi_I(\mathbf{x})\mathbf{u}_I + \sum_{\substack{J \\ n_J \in \mathbf{N}^g}} \phi_J(\mathbf{x})\psi(\mathbf{x})\mathbf{a}_J, \quad (\mathbf{u}_I,\, \mathbf{a}_J \in \mathbb{R}^2) \tag{1}$$

where the nodal set $\mathbf{N}^g$ is defined as:

$$\mathbf{N}^g = \{n_J : n_J \in \mathbf{N},\ \omega_J \cap \Omega_g \neq \emptyset\}. \tag{2}$$

In the above equation, $\omega_J = \mathrm{supp}(n_J)$ is the support of the nodal shape function $\phi_J(\mathbf{x})$, which consists of the union of all elements with n_J as one of its vertices. The choice of the enrichment function $\psi(\mathbf{x})$ for voids and material interfaces will be described in Section 4.

3 The Level Set Method

The level set method (Osher and Sethian, 1988) is a numerical technique for tracking moving interfaces. It is based upon the idea of representing the interface as a level set curve of a higher-dimensional function $\varphi(\mathbf{x}, t)$. In keeping with the applications pursued in this paper, we consider 1-dimensional curves in $\mathbb{R}^2$.

A moving interface $\Gamma(t) \subset \mathbb{R}^2$ can be formulated as the level set curve of a function $\varphi : \mathbb{R}^2 \times \mathbb{R} \to \mathbb{R}$, where

$$\Gamma(t) = \{\mathbf{x} \in \mathbb{R}^2 : \varphi(\mathbf{x}, t) = 0\}. \tag{3}$$

One important example of such a function φ would be the signed distance function:

$$\varphi(\mathbf{x}, t) = \pm \min_{\mathbf{x}_\Gamma \in \Gamma(t)} \|\mathbf{x} - \mathbf{x}_\Gamma\|, \tag{4}$$

where the sign is positive (negative) if $\mathbf{x}$ is outside (inside) the contour defined by $\Gamma(t)$ (we assume that the interface $\Gamma(t)$ is such that one can define an interior and exterior to it).

The evolution of the interface is then embedded in the evolution equation for φ, which is given by (Osher and Sethian, 1988)

$$\varphi_t + F\|\boldsymbol{\nabla}\varphi\| = 0, \tag{5a}$$

$$\varphi(\mathbf{x}, 0) \text{ given,} \tag{5b}$$

where $F(\mathbf{x}, t)$ is the speed of the interface at $\mathbf{x} \in \Gamma(t)$ in the direction of the outward normal to the interface. The key advantages of this method are that it is computed on a fixed Eulerian mesh, handles topological changes in the interface naturally, and can easily be formulated in higher dimensions. Application of the level set method to various problems in engineering and the applied sciences can be found in Sethian (1999).

For our purposes in this paper, the interface is static, so we only use the level set theory for representing the interface. For circular voids, we use

$$\varphi(\mathbf{x}, 0) = \min_{\substack{\mathbf{x}_c^i \in \Omega_c^i \\ i=1,2,\dots,n_c}} \left\{ \|\mathbf{x} - \mathbf{x}_c^i\| - r_c^i \right\}, \tag{6}$$

where Ω_c^i is the domain of the ith void, n_c is the number of circular voids, and $\mathbf{x}_c^i$ and r_c^i are the center and radius of the ith void, respectively.

Consider an elliptical void with semi-major and semi-minor lengths of a and b, respectively, with the axes oriented along the local $\hat{x}_1$ and $\hat{x}_2$-axes, respectively. In addition, let $\hat{\mathbf{e}} = \mathbf{Re}$ be the mapping between the global and the local unit base vectors. Now, the coordinates of a point in the local orthogonal coordinate system with the origin at the center of the ellipse is given by: $\hat{\mathbf{x}} = \mathbf{R}(\mathbf{x} - \mathbf{x}_c)$, where $\mathbf{x}_c$ is the center of the ellipse. Letting $\boldsymbol{\xi} = (\xi_1, \xi_2)$, and $\xi_1 = \hat{x}_1/a$ and $\xi_2 = \hat{x}_2/b$, the equation of the ellipse in the local coordinate system is: $f(\boldsymbol{\xi}) = \|\boldsymbol{\xi}\| - 1 = 0$. Hence a level set function for elliptical voids is given by

$$\Phi(\mathbf{x}, 0) = \min_{i=1,2,\dots,n_e} f(\boldsymbol{\xi}^i), \tag{7a}$$

$$f(\boldsymbol{\xi}^i) = \|\boldsymbol{\xi}^i\| - 1, \tag{7b}$$

$$\boldsymbol{\xi}^i = \left(\frac{\hat{x}_1^i}{a_i}, \frac{\hat{x}_2^i}{b_i} \right), \tag{7c}$$

$$\hat{\mathbf{x}}^i = \mathbf{R}^i(\mathbf{x} - \mathbf{x}_c^i), \tag{7d}$$

where n_e is the number of elliptical voids. Note that in Eq. (7), Φ is a level set function, but not a signed distance function. In order to obtain the signed distance function φ to an elliptical void (interface), one applies the fast marching method to Eq. (9) with $G(\mathbf{x}) = 1$.

Now, consider a polygonal void, whose interface Γ_p ($\Gamma_p = \cup_{i=1}^{p} \mathbf{l}_i$) consists of p segments: $\mathbf{l}_1 = [\mathbf{x}_1, \mathbf{x}_2]$, $\mathbf{l}_2 = [\mathbf{x}_2, \mathbf{x}_3]$, $\dots$, $\mathbf{l}_p = [\mathbf{x}_p, \mathbf{x}_1]$. The level set function for a polygonal interface is given by

$$\varphi(\mathbf{x}, 0) = \|\mathbf{x} - \mathbf{x}_{\min}\| \; sgn\big((\mathbf{x} - \mathbf{x}_{\min}) \cdot \mathbf{n}_{\min}\big), \tag{8a}$$

$$sgn(\xi) = \begin{cases} 1 & \text{if } \xi \geq 0 \\ -1 & \text{if } \xi < 0 \end{cases}, \tag{8b}$$

$$\|\mathbf{x} - \mathbf{x}_{\min}\| = \min_{\substack{\mathbf{x}_i \in \mathbf{l}_i \\ i=1,2,\dots,p}} \|\mathbf{x} - \mathbf{x}_i\|, \tag{8c}$$

where $\mathbf{x}_{\min}$ is the orthogonal projection of $\mathbf{x}$ on the interface Γ_p and $\mathbf{n}_{\min}$ is the outward normal to the interface at $\mathbf{x}_{\min}$. If no unique normal is defined at $\mathbf{x}_{\min}$, the sign is positive if $\mathbf{x} - \mathbf{x}_{\min}$ belongs to the cone of normals at $\mathbf{x}_{\min}$ and negative otherwise.

In Fig. 1, the level set function for a hexagonal interface is shown. For more general interfaces given only as a parameterized curve, the signed distance function is most efficiently calculated using the fast marching method (Sethian, 1996), which optimally solves an equation of the form

$$\|\boldsymbol{\nabla}\varphi\| = \frac{1}{G(\mathbf{x})}, \tag{9}$$

where $G : \mathbb{R}^2 \to \mathbb{R}$ is given. If we take $G(\mathbf{x}) = 1$ and apply the fast marching method to Eq. (9), we can obtain the signed distance function to the interface. This method can be applied to both rectilinear meshes (Sethian, 1999) and also to general triangulated meshes (Barth and Sethian, 1998).

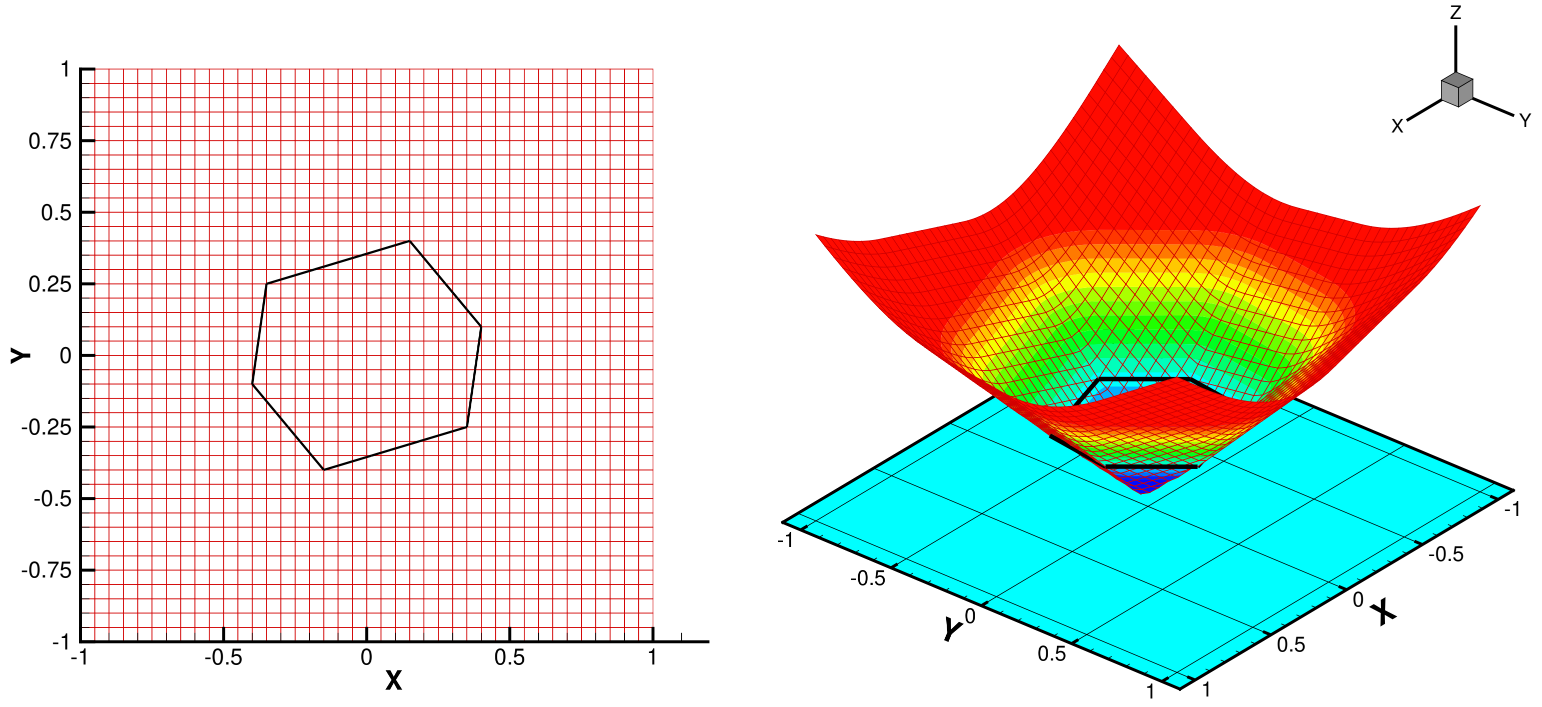

(a)

(b)

Figure 1: Level set function for a hexagonal interface. (a) Mesh, and (b) Level set function.

4 Modeling Voids and Inclusions

Level set methods are used to track the evolution of material interfaces. The geometric description of an interface (for instance, boundary of a hole or inclusion) is represented by the zero level set curve $\varphi \equiv \varphi(\mathbf{x}, t) = 0$. In essence, the physical description of the interface is converted to a discrete functional representation through the function $\varphi(\mathbf{x}, t)$. The geometrical degrees of freedom at a fixed set of points $\mathbf{x}_I$ (nodes) are used to determine φ, and hence the location of the interface. In this study, each finite element node is associated with a geometrical degree of freedom for the level set function. Finite element interpolation is used to compute φ at any point $\mathbf{x}$ in the domain:

$$\varphi(\mathbf{x}) = \sum_I \phi_I(\mathbf{x})\varphi_I, \tag{10}$$

where the summation is over all nodes in the connectivity of the element that contains $\mathbf{x}$, $\phi_I(\mathbf{x})$ are standard finite element shape functions, and φ_I are the nodal values of the level set function. The internal boundaries are then approximately piecewise linear for bilinear quadrilateral elements and exactly linear for three-noded triangular elements.

In the extended finite element method, there is no need to mesh internal boundaries. The computational geometry issues that are associated with the finite element mesh and the internal geometric entities (such as cracks or inclusions) are an important consideration in the X-FEM computations. In light of this, the level set method is an appealing choice that would greatly simplify and speed-up the geometric computations in the X-FEM. In addition, the level set function can also be used to construct enrichment functions within the X-FEM framework. This provides the motivation and seemingly natural choice to use the level set method in conjunction with the extended finite element method.

4.1 Voids

The modeling of voids in the X-FEM is carried out using an enrichment function $V(\mathbf{x})$ for nodes that intersect the boundary of the void. If the node lies outside the void $V(\mathbf{x}) = 1$, and $V(\mathbf{x}) = 0$ if the node is in the interior of the void. In Daux et al. (2000), the discretization of the boundary of the hole was independent of the finite element mesh. The degrees of freedom associated with nodes whose support is entirely inside the void are removed from the system of equations. In the 2-dimensional implementation, instead of using $V(\mathbf{x})$, elements that intersect the boundary of the hole are partitioned such that the weak form is not integrated in the void interior (Daux et al., 2000).

In this work, the point of departure in the modeling of voids lies in using the level set method to represent the voids, and all geometric computations that pertain to the void are carried out using the level set function φ. The level set method provides a convenient and appealing means to model voids with greater flexibility and better computational efficiency. In addition, the finite element mesh and the internal geometric boundary are linked, whereby a self-consistent representation of the internal boundary is obtained for a given finite element mesh.

The computation of the level set function for voids is described in Section 3. For circular voids, the geometrical degrees of freedom indicated in Eq. (10) are evaluated using Eq. (6):

$$\varphi_I = \min_{\substack{\mathbf{x}_c^i \in \Omega_c^i \\ i=1,2,\ldots,n_c}} \left\{ \|\mathbf{x}_I - \mathbf{x}_c^i\| - r_c^i \right\}. \tag{11}$$

4.2 Inclusions

Inclusions are inhomogeneities in a matrix with differing material properties. The modeling of inclusions requires the satisfaction of the Hadamard condition, namely

$$\mathbf{F}^+ - \mathbf{F}^- = \mathbf{a} \otimes \mathbf{n}^+, \tag{12}$$

where $\mathbf{F}$ is the deformation gradient, $\mathbf{n}^+$ is the outward normal to the material interface, and $\mathbf{a}$ is an arbitrary vector in the plane. In Krongauz and Belytschko (1998), a technique for incorporating discontinuities in derivatives for meshless methods was proposed. The use of the level set function φ in the X-FEM provides an elegant and simplified means to achieve the same end. Using $\psi(\varphi)$ as the local enrichment, the X-FEM displacement approximation for two-dimensional domains with inclusions assumes the form:

$$\mathbf{u}^h(\mathbf{x}) = \sum_{\substack{I \\ n_I \in \mathbf{N}}} \phi_I(\mathbf{x})\mathbf{u}_I + \sum_{\substack{J \\ n_J \in \mathbf{N}_\mathrm{I}}} \phi_J(\mathbf{x})\psi\big(\varphi(\mathbf{x})\big)\mathbf{a}_J, \quad (\mathbf{u}_I,\, \mathbf{a}_J \in \mathbb{R}^2) \tag{13}$$

where the nodal set $\mathbf{N}_\mathrm{I}$ is defined as:

$$\mathbf{N}_\mathrm{I} = \{n_J : n_J \in \mathbf{N},\ \omega_J \cap \Gamma_\mathrm{I} \neq \emptyset\}, \tag{14}$$

where Γ_I is the boundary of the inclusion (material interface), and the nodal set $\mathbf{N}$ is defined in Section 2. The enrichment function $\psi\big(\varphi(\mathbf{x})\big) = |\varphi(\mathbf{x})|$ is used in the elements that intersect the material interface, and it is smoothed away from the interface. By construction, since $\varphi_{,n} \neq 0$, the displacement derivatives $u_{i,n}$ are discontinuous across Γ_I.

The level set functions for inclusions follows that which is described in Section 3 for voids. We associate a level set function φ with every distinct material-pair interface (A-B). Hence, all inclusions with interface-pair A_I–B_I are represented by the same level set function, and the number of distinct level set functions is equal to the number of distinct material-pair interfaces. The geometrical degrees of freedom φ_I for circular inclusions are evaluated analogous to that given in Eq. (11).

4.2.1 Nodal Enrichment

The level set function φ is used to develop the local enrichment function for material interfaces. In order to determine the nodes that need to be enriched, the level set function φ is used. We first loop over the elements of the mesh. For a given element, if there exists two nodes n_I and n_J in the connectivity of the element such that $\varphi_I \varphi_J < 0$, we add the element t to the set $\mathbf{T}$ of finite elements that intersect the interface. The enriched nodal set $\mathbf{N}_e$ consists of all nodes that are in the connectivity of the elements in the set $\mathbf{T}$. The above algorithm ensures that if a node belongs to two edges that both lie on the interface, then the node is not enriched. Hence the finite element space is obtained (no enrichment) if the interface lies precisely on element edges.

Let $\psi(\varphi)$ be the enrichment function for a material interface. A first and apparent choice for the enrichment function is: $\psi(\varphi) = |\varphi|$. A second alternative is to take $\psi(\varphi) = |\varphi|$ only in the elements that intersect the interface. Since the enrichment functions exist over the domain of support of the nodes, these enrichment functions are required to be computed one element layer on either side of the elements that intersect the material interface. If $\mathbf{N}_e$ is the set of nodes that are enriched, and φ_I are the level set function values at these nodes, then $\psi_I = \varphi_I$ at these nodes. Let $\mathbf{N}_\psi = \{n_{p+1}, n_{p+2}, \ldots, n_q\}$ be the set of nodes that belong to the adjacent element (outward and inward from the interface), such that $n_I \in \mathbf{N}_\psi$ are sorted in increasing value of the level set function φ. Initially, the value of ψ_I is set to φ_I for the nodes in $\mathbf{N}_\psi$, then we compute a new value for ψ at these nodes based on the following algorithm:

- for $J = p + 1$ to $J = q$
  - create the set $\mathbf{P}_J$, where

    $$\mathbf{P}_J = \{n_I \in \mathbf{N}_e \cup \mathbf{N}_\psi : |\psi_I| < |\varphi_J| \text{ and } n_I,\, n_J \text{ share an edge in the mesh}\}.$$

  - minimize the following expression to obtain ψ_J:

    $$\min \sum_{n_I \in \mathbf{P}_J} \left(\frac{\psi_J - \varphi_I}{L_I} \right)^2, \tag{15}$$

    where L_I is the distance from node n_I to node n_J.
- end for

The solution to the minimization problem in Eq. (15) is explicitly given by

$$\psi_J = \sum_{n_I \in \mathbf{P}_J} \alpha_I \varphi_I, \quad \alpha_I = \frac{\dfrac{1}{L_I^2}}{\sum\limits_{n_K \in \mathbf{P}_J} \dfrac{1}{L_K^2}}, \tag{16}$$

and hence the modified enrichment function is given by

$$\psi(\mathbf{x}) \equiv \psi_1(\mathbf{x}) = \left| \sum_I \phi_I(\mathbf{x}) \psi_I \right|. \tag{17}$$

5 Governing equations

In this section, we present the governing equations of linear elastostatics, together with the weak form and the discrete system for the X-FEM. The case of internal boundaries is considered in the presentation.

5.1 Strong Form

Consider a body which is described by an open bounded domain $\Omega \subset \mathbb{R}^2$, with boundary Γ. The boundary Γ is composed of the sets Γ_u, Γ_t, Γ_h^i and Γ_I^i, such that $\Gamma = \Gamma_u \cup \Gamma_t \cup_{i=1}^m \Gamma_h^i \cup_{i=1}^n \Gamma_I^i$. All the internal holes Γ_h^i are assumed to be traction-free, and traction continuity holds along the material interfaces Γ_I^i. The field equations of elastostatics are:

$$\nabla \cdot \boldsymbol{\sigma} + \mathbf{b} = 0 \quad \text{in} \quad \Omega, \tag{18a}$$

$$\boldsymbol{\sigma} = \mathbf{C} : \boldsymbol{\varepsilon}, \tag{18b}$$

$$\boldsymbol{\varepsilon} = \nabla_s \mathbf{u}, \tag{18c}$$

where ∇_s is the symmetric gradient operator and $\mathbf{C}$ is the tensor of elastic moduli for a homogeneous isotropic material.

The essential and natural boundary conditions are:

$$\mathbf{u} = \bar{\mathbf{u}} \quad \text{on} \quad \Gamma_u, \tag{19a}$$

$$\boldsymbol{\sigma} \cdot \mathbf{n} = \bar{\mathbf{t}} \quad \text{on} \quad \Gamma_t, \tag{19b}$$

$$\boldsymbol{\sigma} \cdot \mathbf{n}_h^i = 0 \quad \text{on} \quad \Gamma_h^i, \quad (i = 1, 2, \ldots, m), \tag{19c}$$

$$[\![\boldsymbol{\sigma} \cdot \mathbf{n}_I^i]\!] = 0 \quad \text{on} \quad \Gamma_I^i, \quad (i = 1, 2, \ldots, n), \tag{19d}$$

where $\mathbf{n}$ is the unit outward normal to Ω, and $\bar{\mathbf{u}}$ and $\bar{\mathbf{t}}$ are prescribed displacements and tractions, respectively.

5.2 Weak Form

Let $\mathbf{u}$ be the displacement solution for the stated elastostatic boundary value problem, with $\boldsymbol{\sigma}(\mathbf{u})$ the corresponding Cauchy stress tensor. Let $\mathbf{u} \in \mathbf{V}$ be the displacement trial solution, and $\mathbf{v} \in \mathbf{V}_0$ be any set of kinematically admissible test functions (virtual displacements). The space $\mathbf{V} = \mathbb{H}^1(\Omega)$ is the Sobolev space of functions with square-integrable first derivatives in Ω, and $\mathbf{V}_0 = \mathbb{H}^1_0(\Omega)$ is the Sobolev space of functions with square-integrable first derivatives in Ω and vanishing values on the essential boundary Γ_u. The weak form of the governing equation and associated boundary conditions can be written as

$$\text{Find } \mathbf{u} \in \mathbf{V} \text{ such that}$$

$$\int_\Omega \boldsymbol{\sigma}(\mathbf{u}) : \boldsymbol{\varepsilon}(\mathbf{v})\, d\Omega = \int_\Omega \mathbf{b} \cdot \mathbf{v}\, d\Omega + \int_{\Gamma_t} \bar{\mathbf{t}} \cdot \mathbf{v}\, d\Gamma \quad \forall\, \mathbf{v} \in \mathbf{V}_0. \tag{20}$$

5.3 Discrete System

Consider the Bubnov-Galerkin implementation for the X-FEM in two-dimensional linear elasticity. In the X-FEM, finite-dimensional subspaces $\mathbf{V}^h \subset \mathbf{V}$ and $\mathbf{V}^h_0 \subset \mathbf{V}_0$ are used as the approximating trial and test spaces. The weak form for the discrete problem can be stated as:

$$\text{Find } \mathbf{u}^h \in \mathbf{V}^h \subset \mathbf{V} \;\text{ such that}$$

$$\int_{\Omega^h} \boldsymbol{\sigma}(\mathbf{u}^h) : \boldsymbol{\varepsilon}(\mathbf{v}^h) = \int_{\Omega^h} \mathbf{b} \cdot \mathbf{v}\, d\Omega + \int_{\Gamma^h_t} \bar{\mathbf{t}} \cdot \mathbf{v}\, d\Gamma \quad \forall\, \mathbf{v}^h \in \mathbf{V}^h_0 \subset \mathbf{V}_0. \tag{21}$$

In a Bubnov-Galerkin procedure, the trial functions $\mathbf{u}^h$ as well as the test functions $\mathbf{v}^h$ are represented as linear combinations of the same shape functions. The trial and test functions are:

$$\mathbf{u}^h(\mathbf{x}) = \sum_I \phi_I(\mathbf{x})\mathbf{u}_I + \sum_J \phi_J(\mathbf{x})\psi\big(\varphi(\mathbf{x})\big)\mathbf{a}_J, \tag{22}$$

$$\mathbf{v}^h(\mathbf{x}) = \sum_I \phi_I(\mathbf{x})\mathbf{v}_I + \sum_J \phi_J(\mathbf{x})\psi\big(\varphi(\mathbf{x})\big)\mathbf{b}_J, \tag{23}$$

where $\phi_I(\mathbf{x})$ are the finite element shape functions, $\varphi(\mathbf{x})$ is the level set function, and $\psi\big(\varphi(\mathbf{x})\big)$ is the enrichment function for a material interface.

On substituting the trial and test functions from Eq. (22) in Eq. (21), and using the arbitrariness of nodal variations, the following discrete system of linear equations is obtained:

$$\mathbf{K}\mathbf{d} = \mathbf{f}, \tag{24}$$

where

$$\mathbf{K}_{IJ} = \int_{\Omega^h} \mathbf{B}_I^T \mathbf{C} \mathbf{B}_J \, d\Omega, \tag{25a}$$

$$\mathbf{f}_I = \int_{\Gamma_t^h} \hat{\phi}_I \bar{\mathbf{t}} \, d\Gamma + \int_{\Omega^h} \hat{\phi}_I \mathbf{b} \, d\Omega, \tag{25b}$$

where $\hat{\phi}_I \equiv \phi_I$ for a finite element displacement degree of freedom, and $\hat{\phi}_I \equiv \phi_I \psi$ for an enriched degree of freedom. In the above equations, $\mathbf{C}$ is the constitutive matrix for an isotropic linear elastic material, and the matrix $\mathbf{B}_I$ is given by

$$\mathbf{B}_I = \begin{bmatrix} \hat{\phi}_{I,x} & 0 \\ 0 & \hat{\phi}_{I,y} \\ \hat{\phi}_{I,y} & \hat{\phi}_{I,x} \end{bmatrix}. \tag{26}$$

6 Numerical Integration

In standard finite element methods, each finite element is associated with a material type; however, in the X-FEM, since internal boundaries of geometric entities do not conform to the mesh, such an association does not exist *a priori*. Using the level set function φ, we can consider two different computational strategies to perform the numerical integration of the weak form. In the first approach, we establish the association between an element or sub-element (partitioned element) and a material type, and use Gauss quadrature rules in each element to carry out the numerical integration. Alternatively, since the material type of a point $\mathbf{x}$ in the domain is known by the sign of $\varphi(\mathbf{x})$, a quad-tree or octree sub-division in 2- and 3-dimensions, respectively, in conjunction with Gauss quadrature, Simpson's rule, or other quadrature rules, is a possible candidate for the numerical integration.

In order to implement the first approach in 2-dimensions, we partition the finite elements that intersect the boundary of the hole or inclusion, into triangles. The level set function φ is used to obtain the 1-dimensional segments of the interface, where each segment sub-divides a finite element $t \in \mathbf{T}$ (see Section 4.2.1) into precisely two domains. An algorithm is implemented to partition a finite element $t \in \mathbf{T}$ that is cut by a segment $[\mathbf{a}, \mathbf{b}]$, where $\mathbf{a}$ and $\mathbf{b}$ lie on the edges of t. The edges of the element t are traversed and if for a particular edge e with nodal connectivity $[n_I^e, n_J^e]$, $\varphi_I^e \varphi_J^e < 0$, then the intersection point $\mathbf{x}_p$ is determined by

$$\mathbf{x}_p = \mathbf{x}_I^e + \xi(\mathbf{x}_J^e - \mathbf{x}_I^e), \quad \xi = -\frac{\varphi_I^e}{\varphi_J^e - \varphi_I^e}. \tag{27}$$

The points $\mathbf{a}$ and $\mathbf{b}$ are found using the above relations. An illustration of the partitioning is depicted in Fig. 2 for an elliptical interface. In Fig. 2, the discretization of the elliptical interface that is realized by the level set computations is shown, along with the partitioned sub-elements on either side of the interface. If the discretized segment of an interface lies along an edge of a finite element, then the element is not partitioned. The above approach is accurate and feasible in 2-dimensions, since

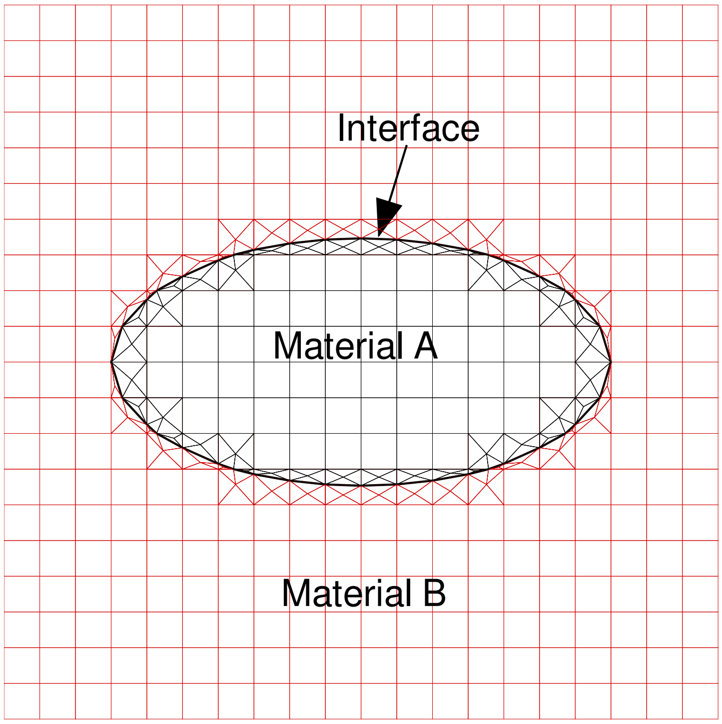

Figure 2: Partitioning and material typing of sub-elements.

the discretization of the interface into linear segments and the partitioning of the finite elements into sub-triangles is readily performed. In 3-dimensions, however, the interface is represented by the union of triangles, and hence the implementation of a partitioning algorithm for the finite elements is non-trivial. In 3-dimensional computations, the second approach we allude to has merit. By an octree sub-division of the finite elements that intersects the interface, and integrating on a given cell if all its vertices lie on the same side of the interface, an easy-to-implement algorithm emerges.

7 Numerical Results

Three problems in 2-dimensional elastostatics are presented to illustrate the accuracy of the new technique. We first solve the problem of an infinite plate with a circular hole under uniaxial tension, and then study two problems of a bimaterial subjected to pure displacement boundary conditions. Since all problems possess an exact solution, a convergence analysis is performed to study the accuracy and rate of convergence of the proposed method. The error in the energy norm that is used in the analysis is defined as:

$$\|\mathbf{u} - \mathbf{u}^h\|_{E(\Omega)} = \left(\int_\Omega (\boldsymbol{\varepsilon} - \boldsymbol{\varepsilon}^h)^T \mathbf{C} (\boldsymbol{\varepsilon} - \boldsymbol{\varepsilon}^h) \, d\Omega \right)^{1/2}. \tag{28}$$

7.1 Infinite Plate with a Circular Hole

An infinite plate with a traction-free circular hole under uniaxial tension ($\sigma_0 = 1$) along x_1 is considered. The exact solution to this problem is given in Szabó and Babuška (1991). In the numerical model, we consider a square domain of edge length L with a circular hole of radius a at its center. We impose the exact tractions on the boundary of the square domain, with appropriate constraints added to remove rigid body modes. The material properties chosen are: Young's modulus $E = 10^5$ and Poisson's ratio $\nu = 0.3$.

In polar coordinates (r, θ), the exact stress distribution for $\sigma_0 = 1$ is given by

$$\sigma_{11}(r,\theta) = 1 - \frac{a^2}{r^2}\left(\frac{3}{2}\cos 2\theta + \cos 4\theta\right) + \frac{3}{2}\frac{a^4}{r^4}\cos 4\theta, \tag{29a}$$

$$\sigma_{22}(r,\theta) = -\frac{a^2}{r^2}\left(\frac{1}{2}\cos 2\theta - \cos 4\theta\right) - \frac{3}{2}\frac{a^4}{r^4}\cos 4\theta, \tag{29b}$$

$$\sigma_{12}(r,\theta) = -\frac{a^2}{r^2}\left(\frac{1}{2}\sin 2\theta + \sin 4\theta\right) + \frac{3}{2}\frac{a^4}{r^4}\sin 4\theta, \tag{29c}$$

where a is the radius of the circular hole. The displacement components are:

$$u_1(r,\theta) = \frac{a}{8\mu}\left[\frac{r}{a}(\kappa+1)\cos\theta + 2\frac{a}{r}((1+\kappa)\cos\theta + \cos 3\theta) - 2\frac{a^3}{r^3}\cos 3\theta\right], \tag{30a}$$

$$u_2(r,\theta) = \frac{a}{8\mu}\left[\frac{r}{a}(\kappa-3)\sin\theta + 2\frac{a}{r}((1-\kappa)\sin\theta + \sin 3\theta) - 2\frac{a^3}{r^3}\sin 3\theta\right], \tag{30b}$$

where μ is the shear modulus and κ (Kolosov constant) is defined as

$$\kappa = \begin{cases} 3 - 4\nu & \text{(plane strain)}, \\ \dfrac{3-\nu}{1+\nu} & \text{(plane stress)}. \end{cases} \tag{31}$$

In the numerical computations, $L = 2$ and plane strain conditions are assumed. A convergence study is carried out using equi-spaced rectangular $L_h \times L_h$ meshes: $L_h = 10, 20, 40, 80, 160$ are used in the computations. The analyses are performed for two different hole radii: $a = 0.3$ and $a = 0.4$. In Fig. 3, the plot of the error in the energy norm versus the mesh spacing is shown on a log–log plot. The rate of convergence (R) in the energy norm is 0.96, which compares well to the optimal rate of one.

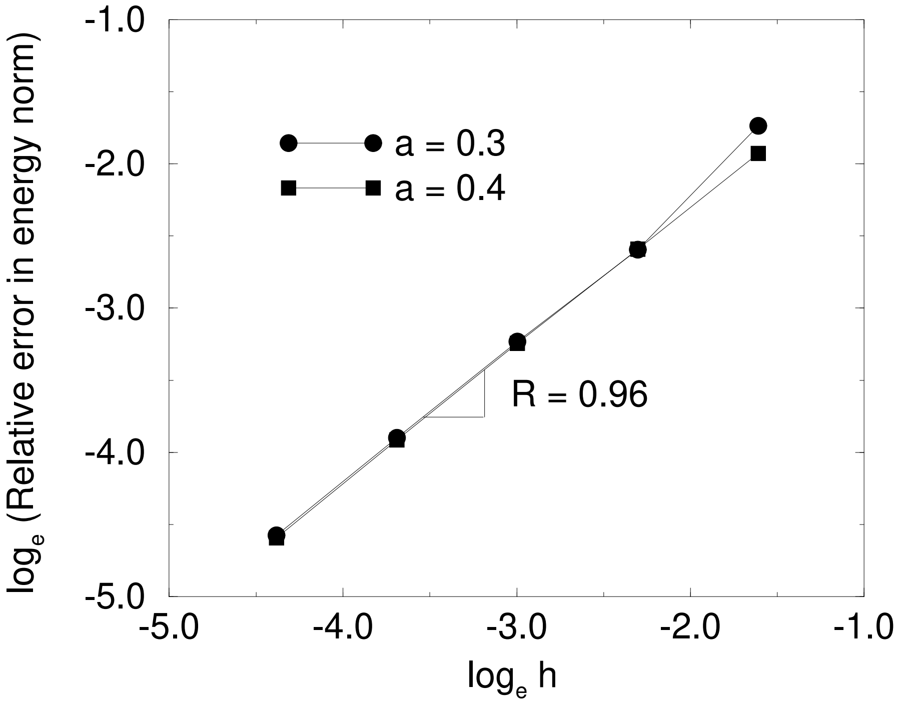

Figure 3: Rate of convergence in energy norm for the plate with a hole problem.

In order to assess the accuracy of the use of level sets in the X-FEM for modeling voids, we compare the finite element solution to that obtained by the new technique for a mesh with approximately the same number of unknowns. The radius of the hole $a = 0.4$. The finite element mesh used consists of 3088 3-noded triangular elements with 1569 nodes (hole explicitly modeled by the mesh), and the corresponding mesh for the X-FEM implementation has 3406 3-noded triangular elements and 1704 nodes (Fig. 4). In Fig. 4, the nodes that are removed from the discrete system are indicated by the dark circles. The number of unknowns in the FE computations is 3135, and that in the X-FEM computations is 3103. A contour plot of the normal stress σ_{11} using the two approaches is presented in Fig. 5. It is seen that the agreement between the results obtained by the two methods is excellent.

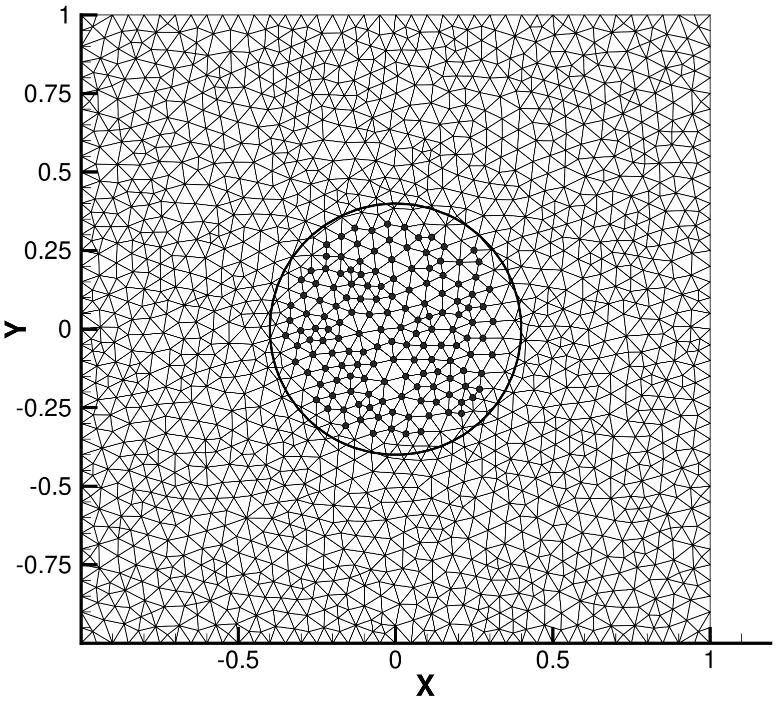

Figure 4: Mesh used in the X-FEM computations.

7.2 Bimaterial Bar

Consider a bimaterial bar ($\Omega = \Omega_1 \cup \Omega_2$) of length $L = 2$ with material moduli E_1 in Ω_1 and E_2 in Ω_2, where $\Omega_1 = (-1, \xi)$ and $\Omega_2 = (\xi, 1)$. The interface $\Gamma_{\rm I}$ is located at $x_1 = \xi$. For the pure Dirichlet problem with $u_1 = 0$ at $x_1 = -1$, $u_1 = 1$ at $x_1 = 1$, and no body forces, the exact displacement solution assumes the form:

$$u_1(x_1) = \begin{cases} (1 + x_1)\alpha & -1 \le x_1 \le \xi \\ 1 + \dfrac{E_1}{E_2}(x_1 - 1)\alpha & \xi \le x_1 \le 1 \end{cases}, \tag{32}$$

where

$$\alpha = \frac{E_2}{E_2(1+\xi) - E_1(\xi - 1)}. \tag{33}$$

In order to explore the appropriate enrichment function for the material interface, we simulate a 1-dimensional bimaterial problem in a 2-dimensional domain. Since the ex-

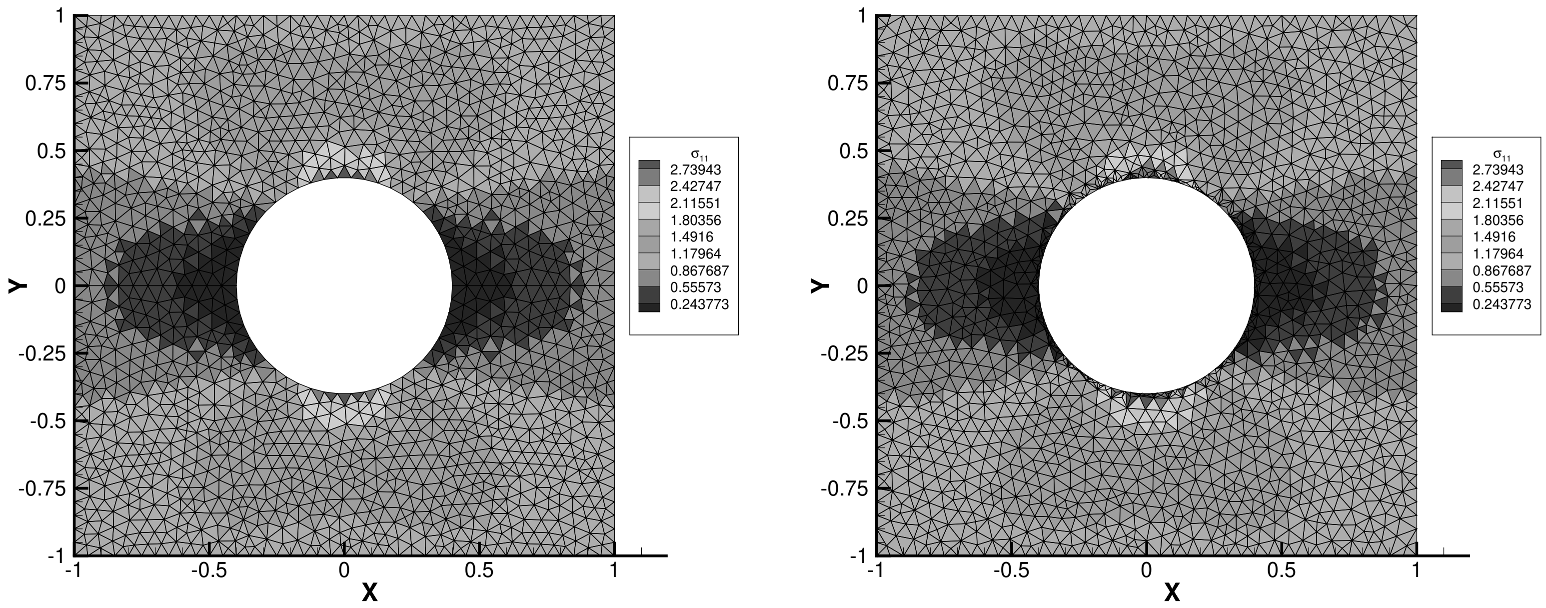

(a)

(b)

Figure 5: Contour plot of the normal stress σ_{11}. (a) FEM; and (b) X-FEM.

act displacement solution is piecewise linear for the bimaterial bar in 1-dimension, we seek an enrichment function for the material interface that preserves the equivalence between the discrete X-FEM space and the discrete FEM space in which the interface is explicitly modeled using finite elements. By analyzing the numerical results for the bimaterial bar problem, we can generalize the enrichment methodology for general curvilinear interfaces in 2-dimensions, with an aim towards accuracy and convergence rate that are on par with finite elements in which the interface is explicitly modeled using elements.

We consider a 2-dimensional domain $\Omega = (-1,1) \times (-1,1)$ with the material interface Γ_{I} located at $\xi \times (-1,1)$. Let the Young's modulus and Poisson's ratio in $\Omega_1 = (-1,\xi) \times (-1,1)$ be $E_1 = 1$, $\nu = 0$, and that in $\Omega_2 = (\xi,1) \times (-1,1)$ be $E_2 = 10$, $\nu = 0$. Numerical results are computed on an equi-spaced 10×10 regular finite element mesh with five different locations of the interface: $\xi = 0.01$, 0.05, 0.1, 0.15, and 0.19. The enrichment functions $\psi = |\varphi|$ and $\psi = \hat{\psi}$ are considered. In Fig. 6a, the finite element mesh and the interface are shown for $\xi = 0.1$, and in Fig. 6b, the enrichment function $\hat{\psi}$ is illustrated. The numerical results for the relative error in the energy norm are presented in Table 1. On using $\psi = |\varphi|$ as the enrichment function, a linear approximation is not obtained in elements that are adjacent to those intersected by the interface. This adversely affects the energy error norm results. However, by using the enrichment function $\hat{\psi}$ shown in Fig. 6b, a linear approximation is obtained in Ω which leads to very accurate results. The numerical results for this model problem indicate that the enrichment function away from the material interface needs to be a constant in order to pass the bimaterial patch test.

7.3 Bimaterial Boundary Value Problem

In Fig. 7, a body composed of two different materials is shown. The material constants are constant in Ω_1 and Ω_2, but there is a discontinuity in the material constants across the interface Γ_1 ($r = a$). The Lamé constants in Ω_1 are chosen as: $\lambda_1 = \mu_1 = 0.4$, and those in Ω_2 are: $\lambda_2 = 5.7692$, $\mu_2 = 3.8461$. These correspond to $E_1 = 1$, $\nu_1 = 0.25$, and $E_2 = 10$, $\nu_2 = 0.3$. We impose the linear displacement field: $u_1 = x_1$, $u_2 = x_2$ ($u_r = r$, $u_\theta = 0$) on the boundary Γ_2 ($r = b$). The Navier's equation in polar coordinates reduces to

$$\frac{d}{dr}\left[\frac{1}{r}\frac{d}{dr}(ru_r)\right] = 0. \tag{34}$$

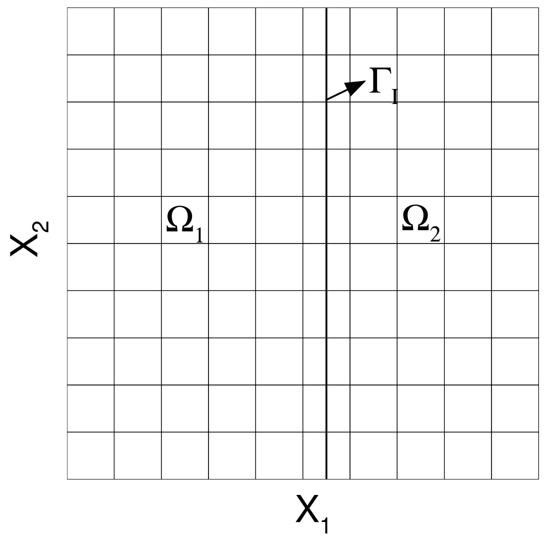

(a)

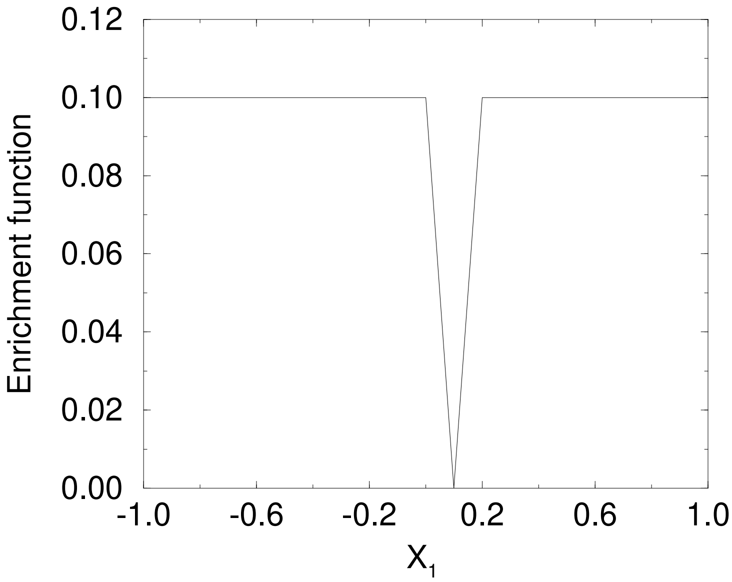

(b)

Figure 6: Bimaterial bar problem. (a) Mesh, and (b) Enrichment function $\hat{\psi}$ ($\xi = 0.1$).

Table 1: Relative error in the energy norms for the bimaterial bar problem.

Interface Location ξ	Enrichment $\lvert\varphi\rvert$	Enrichment $\hat{\psi}$
0.01	8.3×10^{-2}	3.0×10^{-8}
0.05	1.6×10^{-1}	2.8×10^{-8}
0.10	1.8×10^{-1}	2.1×10^{-8}
0.15	1.8×10^{-1}	3.8×10^{-8}
0.19	1.6×10^{-1}	3.6×10^{-8}

By considering displacement and traction continuity across the interface, the exact displacement solution can be written as

$$u_r(r) = \begin{cases} \left[\left(1-\dfrac{b^2}{a^2}\right)\alpha+\dfrac{b^2}{a^2}\right]r, & 0\le r\le a \\ \left(r-\dfrac{b^2}{r}\right)\alpha+\dfrac{b^2}{r} & a\le r\le b \end{cases} \tag{35a}$$

$$u_\theta = 0, \tag{35b}$$

where

$$\alpha = \frac{(\lambda_1+\mu_1+\mu_2)b^2}{(\lambda_2+\mu_2)a^2+(\lambda_1+\mu_1)(b^2-a^2)+\mu_2 b^2}. \tag{35c}$$

The radial (ε_{rr}) and hoop ($\varepsilon_{\theta\theta}$) strains are given by

$$\varepsilon_{rr}(r) = \begin{cases} \left(1-\dfrac{b^2}{a^2}\right)\alpha+\dfrac{b^2}{a^2}, & 0\le r\le a \\ \left(1+\dfrac{b^2}{r^2}\right)\alpha-\dfrac{b^2}{r^2} & a\le r\le b \end{cases} \tag{36a}$$

$$\varepsilon_{\theta\theta}(r) = \begin{cases} \left(1-\dfrac{b^2}{a^2}\right)\alpha+\dfrac{b^2}{a^2}, & 0\le r\le a \\ \left(1-\dfrac{b^2}{r^2}\right)\alpha+\dfrac{b^2}{r^2} & a\le r\le b \end{cases} \tag{36b}$$

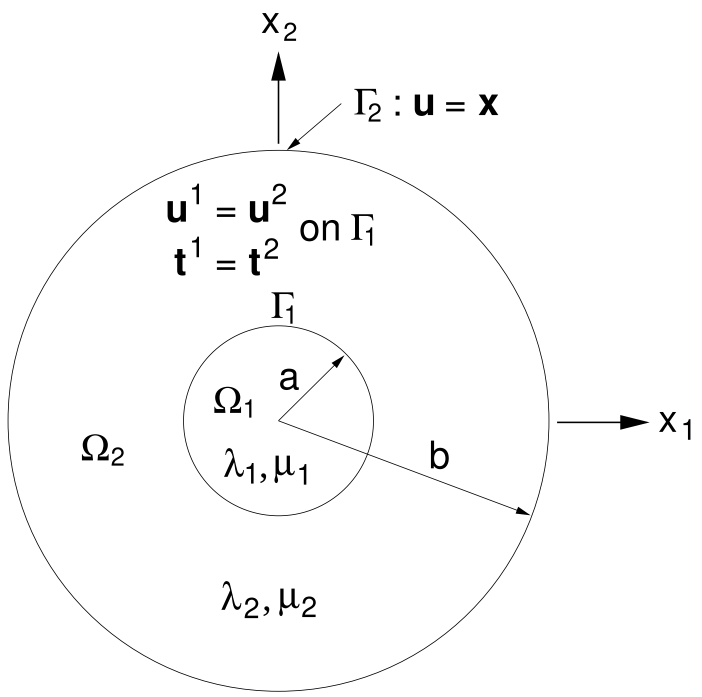

Figure 7: Bimaterial boundary value problem.

and the radial (σ_{rr}) and hoop ($\sigma_{\theta\theta}$) stresses are:

$$\sigma_{rr}(r) = 2\mu\varepsilon_{rr} + \lambda(\varepsilon_{rr} + \varepsilon_{\theta\theta}), \tag{37a}$$

$$\sigma_{\theta\theta}(r) = 2\mu\varepsilon_{\theta\theta} + \lambda(\varepsilon_{rr} + \varepsilon_{\theta\theta}), \tag{37b}$$

where the appropriate Lamé constants are to be used in the evaluation of the normal stresses. The shear components of the stress and strain tensors are zero.

In the numerical model, we consider a square plate ($L \times L$, $L = 2$) with a circular inclusion (Ω_1) of radius $a = 0.4$. On the boundary of the plate, the exact tractions using Eq. (37) are imposed ($a = 0.4$ and $b = 2.0$ are chosen) with appropriate displacement constraints added to remove rigid body modes. A convergence study is conducted using equi-spaced rectangular $L_h \times L_h$ meshes: $L_h = 10$, 20, 40, 80. The finite element computations are carried out using 3-noded triangular elements.

The convergence analysis is carried out for three cases using the X-FEM: (a) No enrichment; (b) Enrichment function $\psi = |\varphi|$; and (c) Enrichment function $\psi = \psi_1$, where ψ_1 is the modified level set function based on the smoothing procedure described in Section 4.2.1. The motivation for the smoothing procedure presented in Section 4.2.1 stems from the numerical experiments conducted in Section 7.2. The enrichment functions for the 20×20 mesh is shown in Fig. 8. In all the above cases, the weak form is integrated appropriately by partitioning the elements that are intersected by the interface. The degrees of freedom of the meshes used in the FEM and in the X-FEM computations are presented in Table 2. The numerical results for the convergence in energy norm are shown in Fig. 9. The accuracy and rate of convergence of the X-FEM with the smoothed form of the enrichment are significantly better than the other two cases. The rate ($R = 0.91$) using the enrichment function ψ_1 is also on par with the optimal rate of unity which is obtained using finite elements with the interface truly modeled by the mesh.

Table 2: Degrees of freedom for the meshes used for the bimaterial problem.

Mesh (h)	FEM	X-FEM (No Enrichment)	X-FEM (Enrichment)
0.2	277	239	287
0.1	915	879	991
0.05	3559	3359	3599
0.025	13693	13119	13615

Even though the enrichment function ψ_1 used in this paper is appropriate from an accuracy and convergence viewpoint, a more general enrichment methodology which would be valid for a wider class of interface problems is attractive. To this end, one can consider the enrichment nodal data ψ_I as also unknowns in the statement of the principle of virtual work (variational form). The nodal data ψ_I are known on nodes that are in the connectivity of the elements that intersect the interface: the modulus of the level set function ($|\varphi|$) is an appropriate choice for this purpose. On elements that are one layer on either side (outer and inner) of these elements, the ψ_I are to be determined by the numerical procedure. As an initial guess, the ψ_I can be set using the smoothing procedure given in Eqs. 15–17. Thereafter, an iterative scheme between the solution of the minimization problem with respect to $\{u_I, a_I\}$ and that with respect to ψ_I would provide the minimization of the global problem. This would result in an optimum choice for ψ_I, and an appropriate form for the enrichment function ψ which is best suited for a given problem.

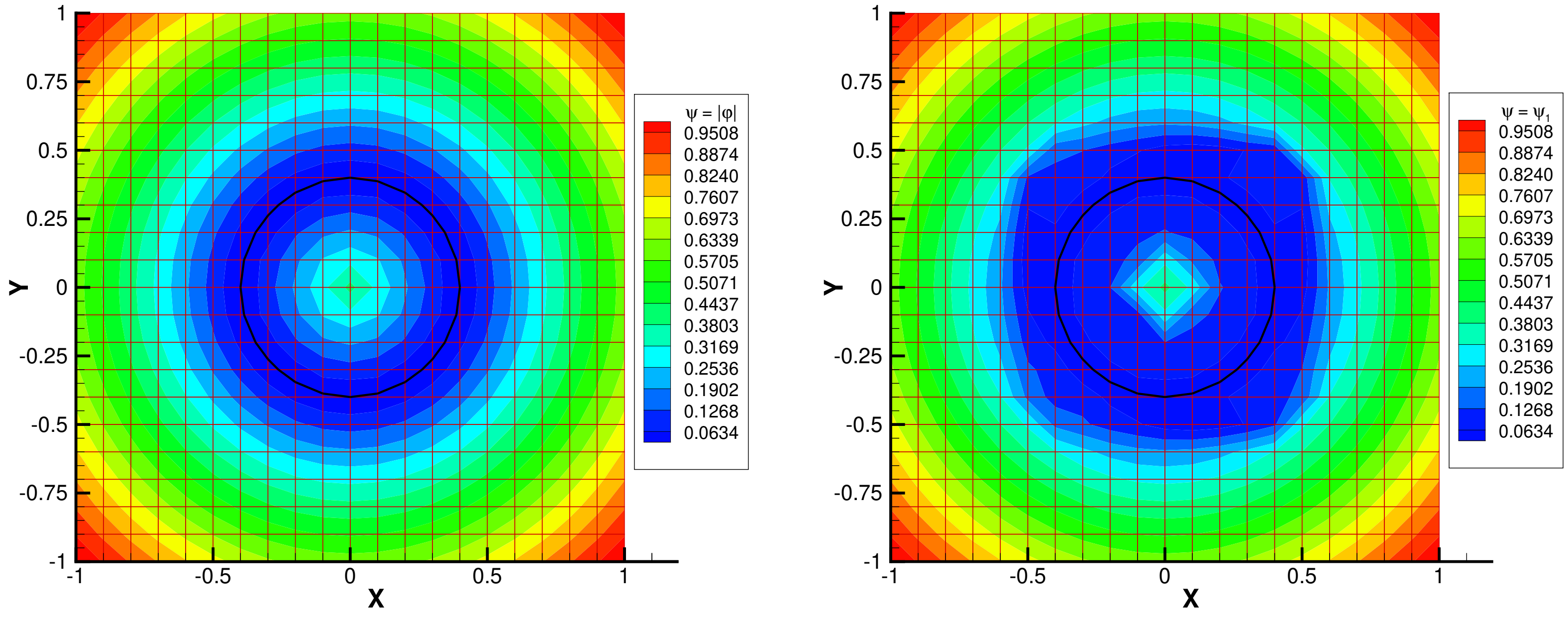

(a) (b)

Figure 8: X-FEM enrichment for material interfaces. (a) $\psi = |\varphi|$, and (b) $\psi = \psi_1$

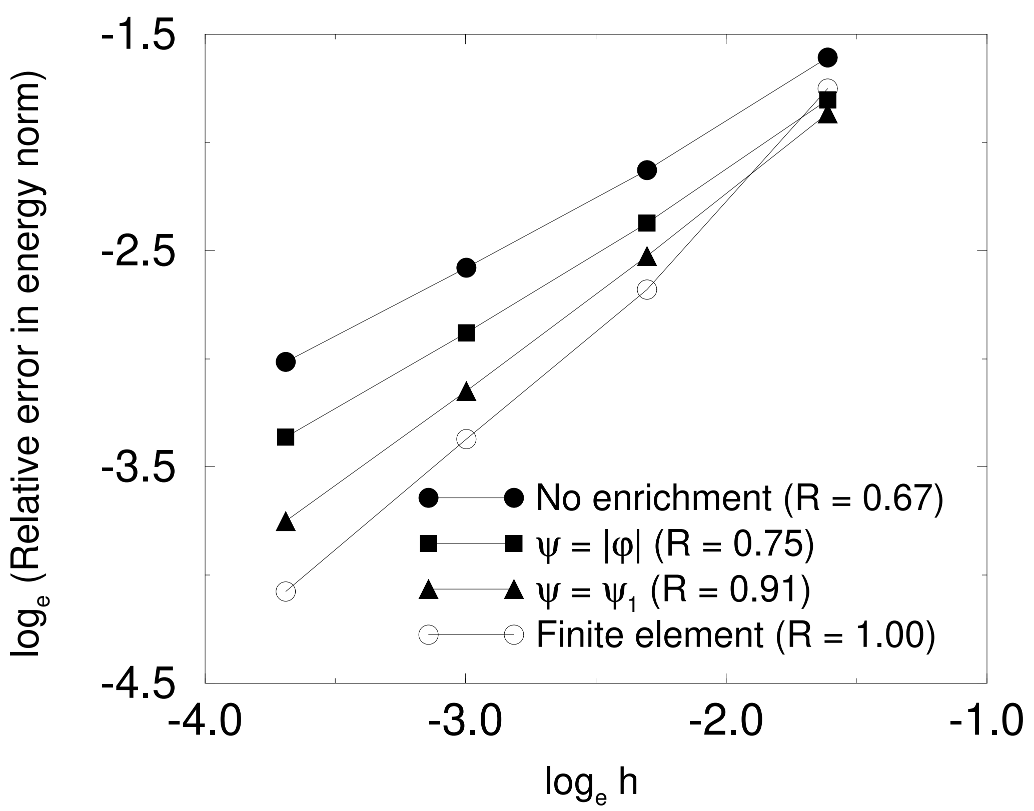

Figure 9: Rate of convergence in energy norm for the bimaterial problem.

8 Conclusions

A methodology to model arbitrary holes and material interfaces (inclusions) without meshing the internal boundaries was proposed. The numerical method couples the level set method (Osher and Sethian, 1988) to the eXtended Finite Element Method (X-FEM) (Moës et al., 1999). In the X-FEM, the finite element space is enriched by adding additional functions to the approximation using the notion of partition of unity. The level set function φ is used to represent holes and inclusions, and in addition, φ is used to develop the local enrichment for material interfaces to model inclusions.

Numerical examples in 2-dimensional linear elastostatics were presented to test the accuracy of the new technique. For the plate with a hole problem, a convergence study was performed for two different radii of the hole. Optimal rate of convergence in energy norm $\big(\mathcal{O}(h)\big)$ was obtained using the new technique. A bimaterial boundary value problem with pure displacement boundary conditions was also considered. Issues pertaining to appropriate choice of enrichment functions for material interfaces were addressed, and a suitable enrichment function was derived that yielded accurate results and near optimal rate of convergence for the 2-dimensional bimaterial problem. This study demonstrated that by incorporating level set functions in the X-FEM, we obtain a powerful and accurate numerical technique for the modeling of voids and inclusions without meshing the internal boundaries. The new technique is simple and versatile, and the results indicate its potential and promise in the modeling of interfacial phenomena in solid and fluid mechanics.

Acknowledgments

The authors are grateful for the research support of the National Science Foundation through contract CMS–9732319, and to the Office of Naval Research and the Army Research Office.

References

Barth, T. J. and J. A. Sethian (1998). Numerical schemes for the Hamilton-Jacobi and level set equations on triangulated domains. *Journal of Computational Physics 145*(1), 1–40.

Daux, C., N. Moës, J. Dolbow, N. Sukumar, and T. Belytschko (2000). Arbitrary cracks and holes with the extended finite element method. *International Journal for Numerical Methods in Engineering 48*(12), 1741–1760.

Dolbow, J., N. Moës, and T. Belytschko (2000). Modeling fracture in Mindlin-Reissner plates with the extended finite element method. *International Journal of Solids and Structures*. in press.

Duarte, C. A., I. Babuška, and J. T. Oden (1998, October). Generalized finite element methods for three dimensional structural mechanics problems. In S. N. Atluri and P. E. O'Donoghue (Eds.), *Modeling and Simulation Based Engineering : Proceedings of the International Conference on Computational Engineering Science*, Volume I, Atlanta, GA, pp. 53–58. Tech. Science Press.

Duarte, C. A., I. Babuška, and J. T. Oden (2000). Generalized finite element methods for three dimensional structural mechanics problems. *Computers and Structures 77*, 215–232.

Krongauz, Y. and T. Belytschko (1998). EFG approximation with discontinuous derivatives. *International Journal for Numerical Methods in Engineering 41*(7), 1215–1233.

Melenk, J. M. and I. Babuška (1996). The partition of unity finite element method: Basic theory and applications. *Computer Methods in Applied Mechanics and Engineering 139*, 289–314.

Moës, N., J. Dolbow, and T. Belytschko (1999). A finite element method for crack growth without remeshing. *International Journal for Numerical Methods in Engineering 46*(1), 131–150.

Oden, J. T., C. A. Duarte, and O. C. Zienkiewicz (1996, December). A new cloud-based *hp* finite element method. Technical Report TICAM Report 96-55, The University of Texas at Austin, Austin, TX, U.S.A.

Oden, J. T., C. A. Duarte, and O. C. Zienkiewicz (1998). A new cloud-based *hp* finite element method. *Computer Methods in Applied Mechanics and Engineering 153*(1–2), 117–126.

Osher, S. and J. A. Sethian (1988, November). Fronts propagating with curvature-dependent speed: Algorithms based on Hamilton-Jacobi formulations. *Journal of Computational Physics 79*(1), 12–49.

Sethian, J. A. (1996). A marching level set method for monotonically advancing fronts. *Proceedings of the National Academy of Sciences 93*(4), 1591–1595.

Sethian, J. A. (1999). *Level Set Methods & Fast Marching Methods: Evolving Interfaces in Computational Geometry, Fluid Mechanics, Computer Vision, and Materials Science*. Cambridge, UK: Cambridge University Press.

Strouboulis, T., I. Babuška, and K. Copps (2000). The design and analysis of the generalized finite element method. *Computer Methods in Applied Mechanics and Engineering 181*(1–3), 43–69.

Strouboulis, T., K. Copps, and I. Babuška (2000). The generalized finite element method : An example of its implementation and illustration of its performance. *International Journal for Numerical Methods in Engineering 47*(8), 1401–1417.

Sukumar, N., D. L. Chopp, and B. Moran (2000). Extended finite element method and fast marching method for three dimensional fatigue crack propagation. *Journal of Computational Physics*. submitted.

Sukumar, N., N. Moës, B. Moran, and T. Belytschko (2000). Extended finite element method for three-dimensional crack modeling. *International Journal for Numerical Methods in Engineering 48*(11), 1549–1570.

Szabó, B. and I. Babuška (1991). *Finite Element Analysis*. New York: John Wiley and Sons.